Far-infrared absorption in triangular and square quantum dots: Characterization of corner and side modes

Manuel Valín-Rodríguez, Antonio Puente, and Llorenç Serra
Departament de Física, Universitat de les Illes Balears, E-07071 Palma de Mallorca, Spain
(Received 1 June 2001; published 26 October 2001)

The far-infrared absorption of triangular and square two-dimensional quantum dots is studied by means of time simulations of the density oscillations within the time-dependent local-spin-density approximation. The absorption is spatially analyzed using a local-response theory that allows the identification of *corner* and *side* modes in the geometric nanostructures. The evolution with a vertical magnetic field of varying intensity is also discussed.

DOI: 10.1103/PhysRevB.64.205307 PACS number(s): 73.21.−b, 72.15.Rn

I. INTRODUCTION

The quantum-dot field has recently focused much attention on the analysis of symmetry unrestricted nanostructures, both from the experimental and theoretical point of view. An important issue is the influence of the dot geometry on the edge modes that manifest in the far-infrared absorption. It is well known that parabolically confined dots can only absorb energy at the frequencies of the confining parabolas (generalized Kohn's theorem[1,2]). However, either departures from a pure radial quadratic law or the introduction of an additional angular dependence in the confining potential may cause the fragmentation of the Kohn modes and the emergence of a more complicated pattern.

At first, the great majority of theoretical approaches to quantum-dot absorption were restricted to the circular symmetry case, solving the random-phase-approximation (RPA) equations by fully exploiting the analytical angular dependence of the single-particle orbitals.[3–5] Although very successful, this scheme is not easily applicable to symmetry-unrestricted nanostructures and different approaches have been proposed. In Ref. 6 Magnúsdóttir and Gudmundsson address the problem within the Hartree theory by solving the resulting RPA matrices in the single-particle basis of the circular problem. The enormous matrix dimensions make the calculation feasible only for a rather small electron number. Alternatively, Ullrich and Vignale[7] have used a perturbative method to describe the absorption of elliptic dots. A different approach was used by two of us in Ref. 8, consisting in the time simulation of the mean-field density oscillations that follow an appropriate initial perturbation and from which one may extract the oscillation frequencies. These *real time* calculations do not rely on any symmetry restriction having also been used to analyze excitations in deformed atomic nuclei and metal clusters.[9,10]

In this work we concentrate on the description of the absorption in triangular and square shaped quantum dots using the time-dependent local-spin-density approximation (TDLSDA). The extension to low magnetic fields within this theory is considered as in Ref. 7. We show that the deformation leads to a departure from the Kohn modes which is peculiar to the shape. At low magnetic fields the spectra possess a rich structure being possible to identify the presence of peak *anticrossings* associated with the deviation from circular shape, similar to those found experimentally by Demel *et al.*[11] To further clarify the origin of the fragmentation, an analysis of the *local* absorption at different points of the nanostructure is given. This allows us to associate each excitation with a particular absorption pattern, thus giving a more physical interpretation of the peaks. In particular, a distinction between *corner* and *side* modes can be established in this way. The magnetic field is shown to introduce an *angular average* of the patterns leading, for increasing intensity, to sizeable shape modifications of the absorption distribution.

Section II of the paper is devoted to the characterization of the ground state for the square and triangular quantum dots. In Sec. III we address the description of the far-infrared absorption presenting in different subsections the formalism and global spectrum (Sec. III A), the local absorption (Sec. III B) and the angular average and magnetic evolution of the absorption patterns (Sec. III C). The conclusions are given in Sec. IV.

II. SYSTEM CHARACTERIZATION

We focus our attention on semiconductor nanostructures of similar sizes and different polygonal shapes, in order to discuss the differences introduced by the geometry. It is assumed that the electron positions are restricted to the xy plane where, in addition, an external potential is confining them to an electronic island. Different shapes are obtained by using the following potential, proposed by Magnúsdóttir and Gudmundsson,[6]

$$V_{ext}(r,\theta)=\frac{1}{2}\omega_0^2 r^2[1+\alpha_p\cos(p\,\theta)], \tag{1}$$

where we have used planar polar coordinates (r,θ) and the standard effective-atomic-unit system.[12] The potential parameter ω_0 gives the parabola curvature while p and α_p determine the deviation from circular symmetry. In this work we shall restrict ourselves to triangular and square shapes. These are the two simplest geometries that deviate from a pure parabolic behavior and whose absorption is therefore not fixed by the generalized Kohn's theorem. A common parabola frequency $\omega_0=0.5$ a.u. has been chosen both for the triangle and square while the deformation parameters

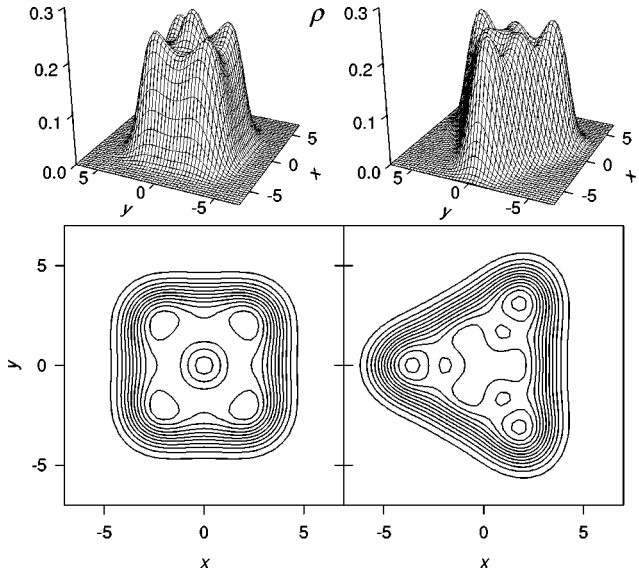

FIG. 1. Density distributions for the square and triangular dots with 12 electrons considered in this work (see Sec. II). Upper plots display the densities as three-dimensional surfaces while lower plots show the corresponding contour lines.

have been fixed to $\alpha_3=0.31$ and $\alpha_4=0.15$ respectively, in order to obtain a proper triangle and box shape, as can be seen in Fig. 1.

We have described the electronic structure within density-functional theory in the LSDA. This approach has been used to address a variety of nonuniform electronic systems—such as atoms, molecules, and clusters—and quantum dots are not an exception for many authors have used this scheme to analyze dot properties.[13–16] Obviously, for our present purposes a symmetry unrestricted solver is required. This can be obtained with different techniques[7,15,16] such as diagonalization in a plane-wave basis or perturbative treatments based on a circular solution. We have resorted to the method developed by two of us in Ref. 8, based on the uniform discretization of the xy plane and the associated transformation of the differential Kohn-Sham equations to be solved with iterative techniques. This method has also been applied by us to the study of quantum rings[17] and dot molecules.[18]

In what follows, we have restricted the present study to nanostructures containing an intermediate number of electrons ($N=12$) for which LSDA is expected to provide a reasonable description of electron-electron interactions. Figure 1 shows that the electronic distribution closely follows the shape of the external potential, clearly of triangular or square form. However, there are also conspicuous density peaks localized either at the corners or the interior of the structure. They are of course attributed to the formation of delocalized electronic orbitals, and to quantum effects associated with the presence of boundaries in the potential, similar to the well-known Friedel oscillations at a metal surface.

III. FAR-INFRARED ABSORPTION

A. Formalism and spectra

The description of excitations in deformed nanostructures constitutes a highly nontrivial task because of the lack of symmetry which does not allow the analytic integration of angular variables as in circular systems. In the present work we have used the TDLSDA to obtain the time evolution, following an initial perturbation, of relevant expectation values. The single-particle orbitals $\{\varphi_i(\mathbf{r})\}$ evolve in time as

$$i\frac{\partial}{\partial t}\varphi_{i\eta}(\mathbf{r},t)=h_\eta[\rho,m]\varphi_{i\eta}(\mathbf{r},t), \tag{2}$$

where $\eta=\uparrow,\downarrow$ is the spin index, and total density and magnetization are given in terms of the spin densities $\rho_\eta(\mathbf{r})=\Sigma_i|\varphi_{i\eta}(\mathbf{r})|^2$, by $\rho=\rho_\uparrow+\rho_\downarrow$ and $m=\rho_\uparrow-\rho_\downarrow$, respectively. The Hamiltonian h_η in Eq. (2) contains, besides kinetic energy, the confining and $v^{(conf)}(\mathbf{r})$, Hartree $v^{(H)}(\mathbf{r})=\int d\mathbf{r}'\rho(\mathbf{r}')/|\mathbf{r}-\mathbf{r}'|$ and exchange-correlation $v_\eta^{(xc)}(\mathbf{r})=(\partial/\partial\rho_\eta)\mathcal{E}_{xc}(\rho,m)$ potentials. The exchange-correlation energy density $\mathcal{E}_{xc}(\rho,m)$ has been described as in Refs. 7 and 8. The Zeeman energy $\pm(1/2)g^*\mu_B B$ (Ref. 19) is also included in Eq. (2).

An initial perturbation of the ground-state orbitals $\varphi'(\mathbf{r})=\mathcal{P}\varphi(\mathbf{r})$ models the interaction with the external field. For dipole excitations, corresponding to far-infrared (FIR) absorption in nanostructures, the unitary operator $\mathcal{P}$ is represented by a rigid translation in an arbitrary direction $\hat{\mathbf{e}}$, specifically

$$\mathcal{P}=\exp[i\lambda\hat{\mathbf{e}}\cdot\mathbf{p}], \tag{3}$$

where the λ parameter has been taken small enough in order to keep the system response in the linear regime. After the initial excitation we keep track of $\langle\mathbf{r}\rangle(t)$ from where a frequency analysis provides the absorption energies and their associated intensities,[8] characterized by the strength function $S_{\hat{\mathbf{e}}}(\omega)$,

$$\mathcal{D}_{\hat{\mathbf{e}}}(\omega)=\hat{\mathbf{e}}\cdot\int dt\, e^{i\omega t}\langle\mathbf{r}\rangle(t),$$

$$S_{\hat{\mathbf{e}}}(\omega)=|\mathcal{D}_{\hat{\mathbf{e}}}(\omega)|. \tag{4}$$

Usually, one is interested in an average over different oscillation directions, corresponding to the absorption of nonpolarized radiation. This implies to average Eq. (4) over all $\hat{\mathbf{e}}$ directions. Taking into account that in the small amplitude limit the strength in a particular direction only depends on the initial amplitude given in that direction the averaged strength may be obtained as[20]

$$S_{av}(\omega)\equiv\frac{1}{2\pi}\int_0^{2\pi}d\theta\, S_{\hat{\mathbf{e}}}(\omega)=\frac{1}{2\pi}\int_0^{2\pi}d\theta|\cos(\theta)^2\mathcal{D}_x(\omega)+\sin(\theta)^2\mathcal{D}_y(\omega)|. \tag{5}$$

It can easily be shown that for geometries with two or more equivalent symmetry axes $S_{\hat{\mathbf{e}}}(\omega)$ actually does not depend on $\hat{\mathbf{e}}$ and therefore it coincides with $S_{av}(\omega)$.

Figure 2 displays the averaged spectrum obtained at $B=0$ for the square and triangle. Notice that both cases show a two peak spectrum within LSDA, although the interpeak separation is much higher for the triangle than for the square.

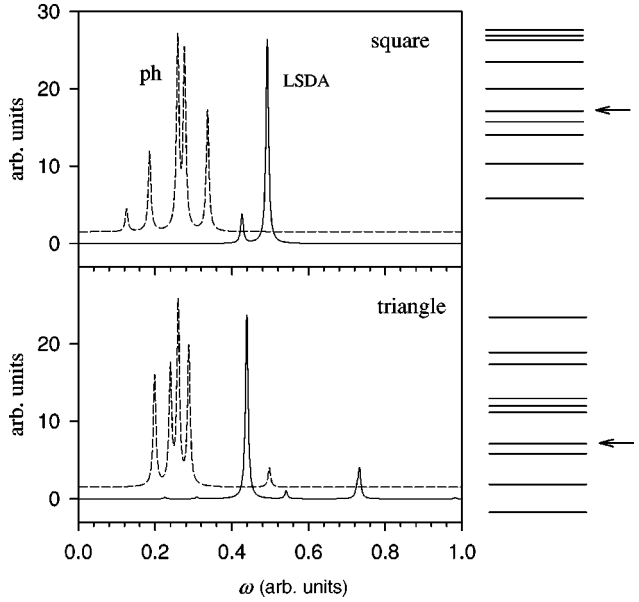

FIG. 2. Absorption spectra for the square and triangle. The solid line corresponds to the TDLSDA while the dashed line shows the noninteracting response. For clarity the noninteracting response has been slightly shifted in the vertical direction. The right plots show the relative position of the lowest energy levels in each case with the arrow indicating the position of the highest-occupied orbital.

This can be attributed to the higher level separation in the triangle. In fact, in the triangular case the single-particle levels exhibit a shell-like structure with gaps between groups of close levels, while for the square level straggling is somewhat higher. This reflects in the distribution of particle-hole transitions also shown in Fig. 2.

The evolution of the absorption spectra with the intensity of the static magnetic field is shown in Fig. 3. In general, the magnetic field induces a splitting of the $B=0$ peaks, as is well known for the circular parabola[2] where the two frequencies are $\omega_{\pm}=\sqrt{\omega_0^2+\omega_c^2/4}\pm\omega_c/2$. For the square and triangular dots the situation is more involved, since the *B*-induced splitting goes along with geometry effects. Figure 3 indicates that there is a repulsion amongst the branches that originate from the $B=0$ modes, showing a zone of avoided crossings or *anticrossings* of the collective peaks. These anticrossing areas are very sensitive to the geometry, showing complicated patterns with more than just two peaks. Indeed, for the square it roughly covers the interval 0.3–0.7 T while for the triangle this region is more extended lying between 0.5 and 2 T. A similar difference is found when comparing the magnetic field B_{pol} at which the ground-state spin polarizes from $S=0$ to $S=1$. The square first transition lies at $B_{pol}=0.5$ T while for the triangle it is $B_{pol}=2.7$ T. We also notice that the minimum-energy gap between the two main branches is much smaller for the square than for the triangle.

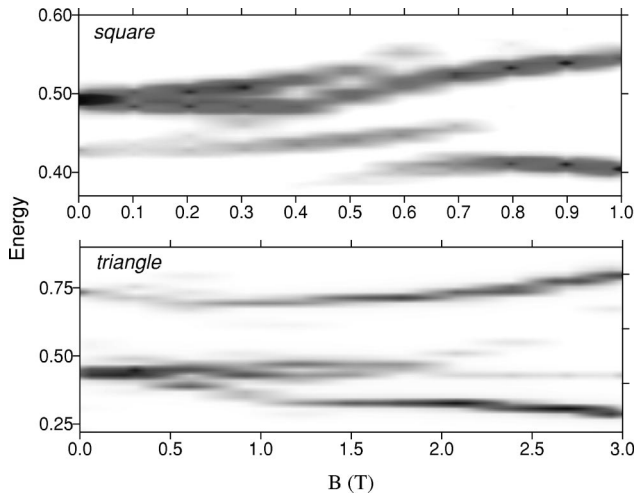

FIG. 3. Magnetic-field evolution of the absorption spectrum of the square and triangle shown in a gray color scale, with black and white indicating high and low absorption levels, respectively.

B. Local absorption

To further analyze the origin of the fragmented absorption in squares and triangles we have computed the *local* absorption in a way similar to that used in Ref. 21 in the context of excitonic states in semiconductors. This technique allows us to study the global absorption spectrum taking into account the different contributions from each spatial point, depending on how the electronic density is oscillating in time in the

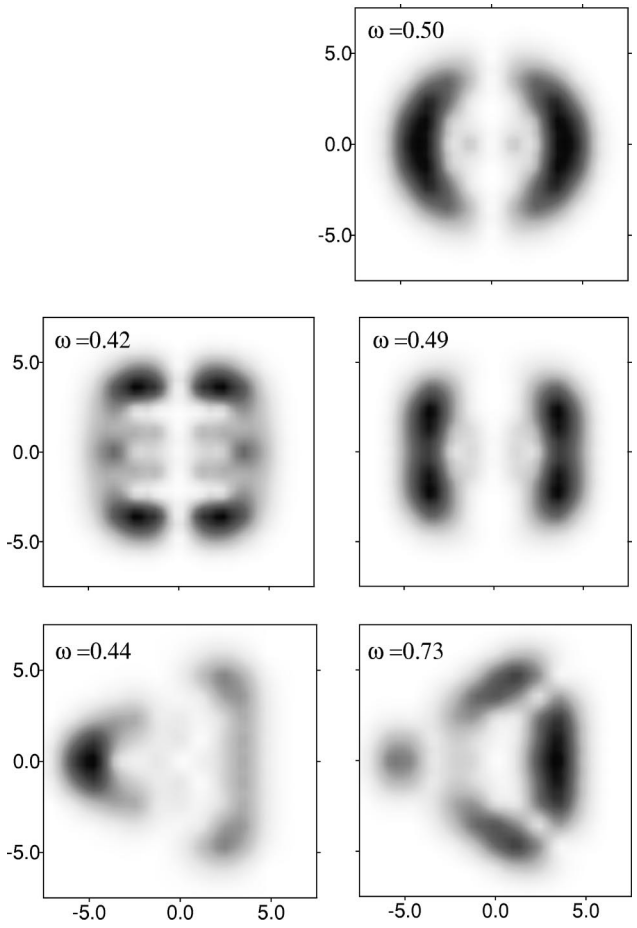

FIG. 4. Local absorption patterns in the circle, square, and triangle for an oscillation along the *x* axis and the energies indicated in each panel.

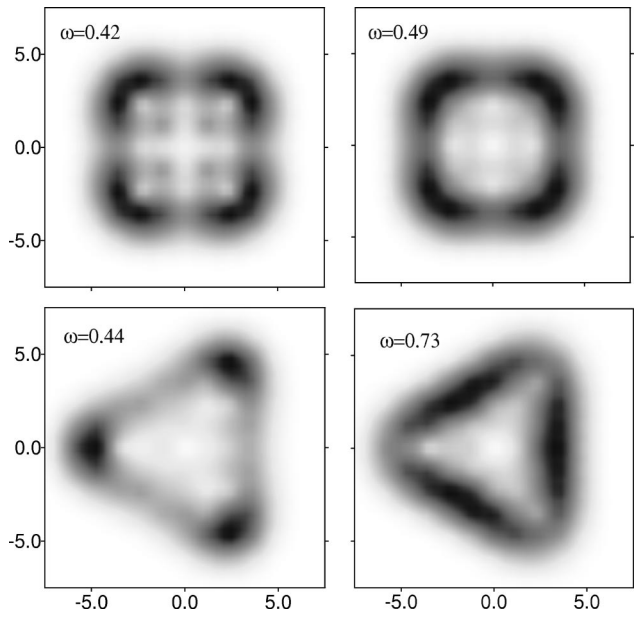

FIG. 5. Average over polarization directions of the same modes of Fig. 4 obtained by switching on an small vertical magnetic field.

vicinity of that point. In practice, we simulate this position-dependent probe by introducing a local weighting function (a narrow Gaussian centered on each point) and look for the oscillation frequencies of the convoluted density as a function of the probe position. After an initial dipole perturbation each local signal will evolve differently in time, thus manifesting the differences in absorption on a local scale. Figure 4 shows the local absorption for the two modes at $B=0$ of the square and triangle when the system is excited along the x axis ($\hat{\mathbf{e}}=\hat{\mathbf{x}}$). As a reference we also show the circular parabolic case, namely, $\alpha_p=0$ in Eq. (1).

The density in a circular parabola oscillates rigidly at the parabola frequency (Kohn's theorem) and from Fig. 4 we notice that the absorption indeed localizes on the edges along

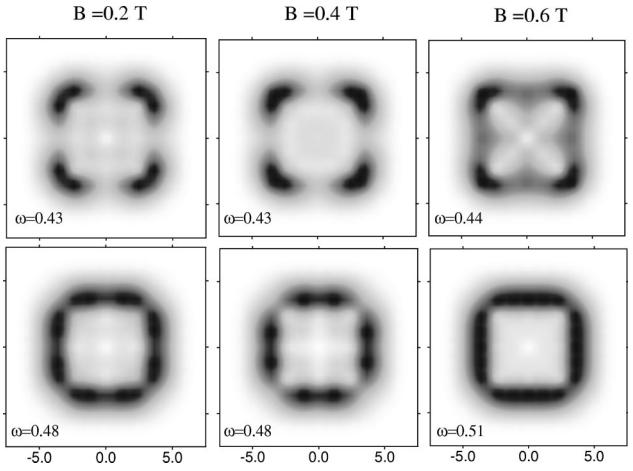

FIG. 6. Magnetic-field evolution of selected absorption patterns within the anticrossing region of the square dot. The magnetic field and energy allow us to exactly identify what mode of Fig. 3 is being considered in each case.

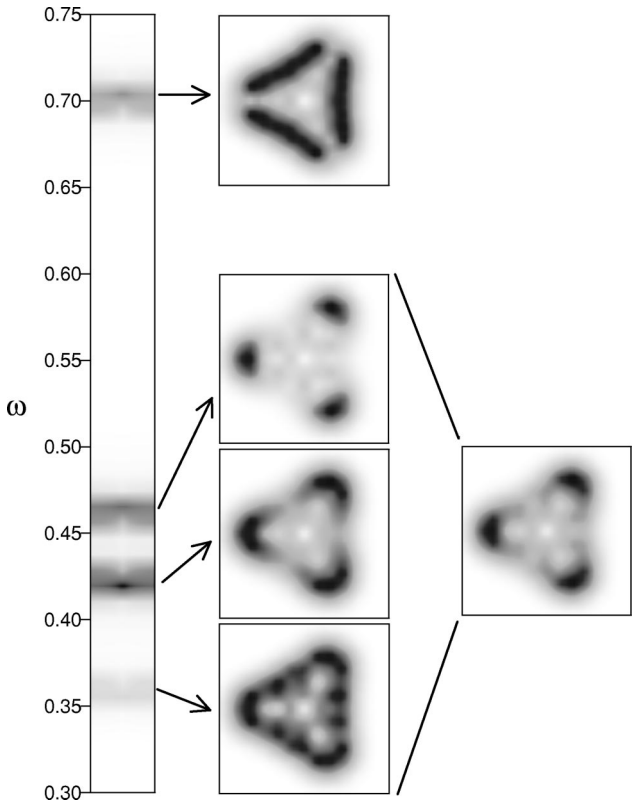

FIG. 7. Spatial absorption patterns corresponding to different modes of the triangular nanostructure for $B=1$ T. The arrows join each spatial pattern to its corresponding excitation energy in the spectral interval. See text for more details.

the oscillation direction (x axis), as was to be expected. Turning now to the square geometry we notice that the dominant mode at $\omega=0.49$, very close to the parabola frequency $\omega_0=0.5$, spatially localizes along the edges in the polarization direction in a way quite similar to the circular case. On the contrary, the lower square mode at $\omega=0.42$ very clearly deviates from this situation showing four maxima at the corners of the nanostructure. This result suggests a classification of the two excitations as *side* and *corner* modes, respectively. This classification is confirmed in the case of the triangle, where we see that the $\omega=0.73$ mode basically absorbs on one of the triangle sides while the $\omega=0.44$ absorbs on the opposite corner. The distinction between side and corner modes will be further commented on in the next subsection where we shall present the angular average of the absorption patterns.

A remarkable property seen in Fig. 4 regards the spatial self-organization of the absorption modes. Indeed, we realize that both in the square and the triangle the absorption maxima for a given mode lie at regions where the absorption for the other mode is strongly quenched. We may interpret this as a *mode competition* for an efficient distribution over the available nanostructure surface.

C. Magnetic-field dependence

The magnetic field introduces a Coriolis-like force that makes the oscillation axis rotate in time. As a consequence,

the initial chosen direction becomes unimportant since the magnetic field will automatically change it in time. We can take advantage of this effect to obtain the averaged absorption patterns of Fig. 4 over polarization directions by switching on a very small magnetic field. Figure 5 shows the angularly averaged patterns corresponding to the same modes displayed in Fig. 4. The distinction between corner and side modes is very clear in the case of the triangle: for $\omega=0.44$ the mode is of corner type and for $\omega=0.73$ it is of side character. For the square this distinction is not as clear because the corners always absorb more than the side centers. Nevertheless, the corner character is somehow higher for the low energy mode $\omega=0.42$ than for the high $\omega=0.49$ one; in fact the former shows vanishing absorption at the side centers while the latter has a much smoother angular dependence.

When the magnetic field is increased additional fragmentation, with a complicated distribution of the absorption, appear both in the square and the triangle (cf. Fig. 3). Because of the very large number of possible cases, we shall only select the more illustrative examples in the anticrossing areas. Our aim is to discern the absorption pattern evolution with applied magnetic field and in particular, to check whether there is a relation between the energy repulsion of modes and their spatial localization. Figures 6 and 7 show the evolution with B of the pattern for the two branches with the higher absorption, that repel each other, in the square and triangular dot, respectively. We see in Fig. 6 that indeed for the square a clear localization takes place at $B=0.4$ T (the center of the anticrossing region) at the corners for the low-energy branch and at the sides for the high-energy one. In the triangle, a more conspicuous side and corner character of the branches is retained for all magnetic fields due, as discussed above, to the existence of a greater energy gap between the different modes. Figure 7 shows the patterns for $B=1$ T as well as the corresponding energy in the spectral range. The three lower patterns give rise, when added according to their relative strength, to the global strength distribution displayed in the right-most panel which exhibits a clear corner identity. Conversely, the upper branch possess a markedly side character. The same trends have been obtained in the full range of magnetic fields corresponding to Fig. 3 for the triangle.

IV. CONCLUSIONS

The FIR absorption of a quantum dot with a triangular or square shape has been analyzed taking into account the effect of an applied static magnetic field, by means of real-time simulations in a spatial mesh within the LSDA formalism. The fragmentation of the absorption due to the noncircular shape has been emphasized. In particular, the existence of a rich absorption distribution for intermediate magnetic fields, associated with the repulsion between modes in the so-called anticrossing energy interval has been analyzed.

The absorption pattern corresponding to the several excitation modes, for a given magnetic field, has been obtained from the local-density oscillations. These patterns allow us to easily interpret the physical character of each mode. In particular, we have identified the existence of corner and side modes in the nanostructure. In the anticrossing intervals the absorption patterns of different modes do not significantly overlap, a result that we attribute to a mode competition for the available dot surface as well as a mode spatial repulsion, consistent with the energy repulsion leading to the anticrossing effect.

ACKNOWLEDGMENT

This work was supported by the Spanish DGESeIC, Grant No. PB98-0124.

[1] L. Brey, N. F. Johnson, and B. I. Halperin, Phys. Rev. B **40**, 10 647 (1989).
[2] P. A. Maksym and T. Chakraborty, Phys. Rev. Lett. **65**, 108 (1990).
[3] D. A. Broido, K. Kempa, and P. Bakshi, Phys. Rev. B **42**, 11 400 (1990).
[4] V. Gudmundsson and R. R. Gerhardts, Phys. Rev. B **43**, 12 098 (1991); V. Gudmundsson and J. J. Palacios, *ibid.* **52**, 11 266 (1995).
[5] Ll. Serra and E. Lipparini, Europhys. Lett. **40**, 667 (1997); Ll. Serra, M. Barranco, A. Emperador, M. Pi, and E. Lipparini, Phys. Rev. B **59**, 15 290 (1999).
[6] I. Magnúsdóttir and V. Gudmundsson, Phys. Rev. B **60**, 16 591 (1999).
[7] C. A. Ullrich and G. Vignale, Phys. Rev. B **61**, 2729 (2000).
[8] A. Puente and Ll. Serra, Phys. Rev. Lett. **83**, 3266 (1999).
[9] H. Flocard, S. E. Koonin, and M. S. Weiss, Phys. Rev. C **17**, 1682 (1978).
[10] K. Yabana and G. F. Bertsch, Phys. Rev. B **54**, 4484 (1996); L. Mornas, F. Calvayrac, E. Suraud, and P.-G. Reinhard, Z. Phys. D: At., Mol. Clusters **38**, 73 (1996).
[11] T. Demel, D. Heitmann, P. Grambow, and K. Ploog, Phys. Rev. Lett. **64**, 788 (1990).
[12] We use $\hbar=m=e^2/\kappa=1$, which for the GaAs effective mass ($m=0.067m_e$) and dielectric constant $\kappa=12.4$ imply an energy and length units of ≈ 12 meV and ≈ 97 Å, respectively.
[13] M. Ferconi and G. Vignale, Phys. Rev. B **50**, 14 722 (1994).
[14] M. Pi, M. Barranco, A. Emperador, E. Lipparini, and Ll. Serra, Phys. Rev. B **57**, 14 783 (1998).
[15] M. Koskinen, M. Manninen, and S. M. Reimann, Phys. Rev. Lett. **79**, 1389 (1999).
[16] K. Hirose and N. S. Wingreen, Phys. Rev. B **59**, 4604 (1999).
[17] M. Valín-Rodríguez, A. Puente, and Ll. Serra, Eur. Phys. J. D **12**, 493 (2000).
[18] M. Valín-Rodríguez, A. Puente, and Ll. Serra, Proceedings of the ISSPIC10 conference, Eur. Phys. J. D (to be published).
[19] μ_B denotes the Bohr magneton and g^* the effective gyromagnetic factor which in bulk GaAs takes a value of -0.44.
[20] A. Puente and Ll. Serra, Europhys. Lett. **55**, 73 (2001).
[21] C. D. Simserides, U. Hohenester, G. Goldoni, and E. Molinari, Phys. Rev. B **62**, 13 657 (2000); O. Mauritz, G. Goldoni, E. Molinari, and F. Rossi, *ibid.* **62**, 8204 (2000).